ACCSCIENCE PUBLISHING

International Journal of Bioprinting

RESEARCH ARTICLE

Digital light processing-printed macroencapsulated human liver organoids preserve hepatic stellate cell quiescence for transplantation in immunocompetent mice

Zhi Zhou[1†], Ruitong Li[1†], Xiaodong Ding[1], Yixuan Li[1], Yixue Luo[2*], and Shaojun Liang[1*]

[1]Tianjin Key Laboratory of Life and Health Detection, Life and Health Intelligent Research Institute, School of Materials Science & Engineering, Tianjin University of Technology, Tianjin, China

[2]Biomanufacturing and Rapid Forming Technology Key Laboratory of Beijing, Department of Mechanical Engineering, School of Mechanical Engineering, Tsinghua University, Beijing, China

[†]*These authors contributed equally to this work.*

***Corresponding authors:**
Shaojun Liang
(liangshaojun@email.tjut.edu.cn)
Yixue Luo
(18810763258@163.com)

Citation: Zhou Z, Li R, Ding X, Li Y, Liang S. Digital light processing-printed macroencapsulated human liver organoids preserve hepatic stellate cell quiescence for transplantation in immunocompetent mice. *Int J Bioprint.* 2026;12(3):026140130. doi: 10.36922/IJB026140130

Received: April 5, 2026

Revised: May 14, 2026

Accepted: May 22, 2026

Published online: May 22, 2026

Abstract

Digital light processing (DLP) bioprinting enables the fabrication of stem cell-derived liver organoids into biomimetic architectures. However, preserving quiescent hepatic stellate cells (HSCs) within human liver organoids during DLP printing remains challenging, as the mechanical requirements for print fidelity often conflict with the compliant microenvironment necessary for maintaining HSC quiescence. To address this limitation, we delineated the printable window of induced pluripotent stem cell (iPSC)-derived HSCs that balances printability with resistance to activation. Notably, day 10 HSCs retained a quiescent phenotype, contributing to the assembly of multicellular organoids without fibrotic activation. We subsequently evaluated the stress-relaxation properties of poly(ethylene glycol) diacrylate (PEGDA)–gelatin methacryloyl (GelMA) and F127DA–GelMA hydrogels, demonstrating that fast-relaxing inner hydrogels preserved the compact cellular morphology of liver organoids, suppressed activation-associated gene expression, and protected HSCs from fibrotic conversion. This highlights that stress relaxation, rather than stiffness alone, is critical for cellular adaptation. Then, we developed a DLP-bioprinted macroencapsulation platform integrating stage-selected iPSC-derived HSCs, stress relaxation-tuned hydrogels, and a protective outer shell. The DLP-printed outer shell conferred structural integrity to the macroencapsulated construct, enabling successful implantation in immunocompetent mice with high graft viability and minimal alpha-smooth muscle actin (α-SMA) expression in iPSC-derived liver organoids containing HSCs. In summary, this study establishes a coordinated strategy harmonizing HSC selection, matrix mechanics, and bioprinting design to balance biological and mechanical demands, yielding structurally stable, physiologically relevant liver organoids while preventing fibrotic activation during biofabrication.

Keywords: Human liver organoids; Hepatic stellate cells; Digital light processing bioprinting; Stress relaxation; Macroencapsulation

1. Introduction

Human liver organoids (LOs) have emerged as promising in vitro models for studying liver development, disease, and regeneration, as they can partially recapitulate hepatic architecture, multicellular composition, and tissue function.[1-4] Within the cellular components of LOs, hepatic stellate cells (HSCs) are critical non-parenchymal liver cells that contribute to hepatic homeostasis and regulate liver zonation, size, and tissue function.[5] In their quiescent state, HSCs store vitamin A and maintain a normal hepatic microenvironment, whereas upon activation, they lose these features, acquire a myofibroblast-like phenotype, and promote extracellular matrix deposition and fibrogenesis.[6] This transition shifts the LOs away from a physiological baseline toward a fibrosis-like state. Accordingly, preservation of a quiescent or low-activation HSC state is important for human LOs that faithfully represent normal liver physiology rather than a pre-fibrotic condition. However, primary human HSCs are scarce and readily undergo spontaneous activation during isolation and in vitro expansion, thereby limiting their utility in standardized tissue models.[7] Human induced pluripotent stem cell (iPSC)-derived HSCs provide a renewable and controllable alternative and have been used for fibrosis modeling and drug screening.[8]

Three-dimensional bioprinting offers LOs a defined mechanical microenvironment and a controlled geometric architecture, enabling the recapitulation of native hepatic tissue structure.[9,10] In particular, digital light processing (DLP)-based bioprinting exhibits practical advantages, including rapid fabrication, high structural fidelity, and relatively low shear stress during processing[9,11,12], rendering it particularly suitable for replicating the hierarchical architecture of native organs while providing mechanical protection for sensitive cell populations during transplantation.[13,14] However, current DLP hydrogel formulations often prioritize matrix stiffness to ensure printing fidelity and fabrication efficiency[15], potentially compromising the maintenance of HSC quiescence within LOs, given the pronounced mechanosensitivity of these cells and their propensity to activate upon matrix stiffening.[6] Therefore, the fabrication of structurally and functionally biomimetic LOs via DLP bioprinting necessitates consideration of the mechanical compatibility between the printed hydrogel matrices and the mechanosensitivity of HSCs.

Here, we established a DLP-printable human LO platform that preserved HSC quiescence and enabled transplantation in immunocompetent mice. We achieved the maintenance of quiescence in printed LOs through the optimization of both the printable window for iPSC-derived HSCs and the mechanical properties of DLP-printed hydrogel matrices. Subsequently, we employed DLP bioprinting to fabricate a macroencapsulated construct comprising an organoid-compatible inner matrix encased within a DLP-bioprinted outer shell, yielding stable and viable grafts devoid of fibrotic activation. This study establishes a biofabrication framework for generating and transplanting LOs that preserves the quiescent phenotype of HSCs.

2. Materials and methods

2.1. Differentiation of induced pluripotent stem cells to hepatic stellate cells, endothelial cells, and hepatoblasts

Human iPSCs (RC01001-A, Nuwacell, China) were cultured with ncTarget medium (RP01020, Nuwacell). When the cells reached approximately 80% confluence, subculture was carried out at a ratio of 1:10.

For HSC differentiation, iPSCs were sequentially induced through mesodermal, mesenchymal/mesothelial, and HSC specification stages, as outlined in Figure 1A, following an adapted protocol based on Coll *et al.*[7] Mesoderm induction was performed from day 0 to day 4 in basal medium supplemented with bone morphogenetic protein 4 (BMP4; 96-120-05, PeproTech, United States [US]), followed by mesenchymal/mesothelial patterning from day 4 to day 8 using BMP4, fibroblast growth factor 1 (FGF1; 100-17A, PeproTech), and FGF3 (558004, BioLegend, US), with retinol (R7632-100MG, Sigma-Aldrich, US), palmitic acid (P0500, Sigma-Aldrich), and B27 minus insulin (A1895601, Gibco, US) added from day 6. Cells were subsequently matured toward an HSC-like fate from day 8 to day 12 in MCDB-201 basal medium (M6770, Sigma-Aldrich) containing retinol, palmitic acid, and B27 minus insulin.

For endothelial differentiation, human iPSCs were seeded onto Matrigel-coated plates, cultured overnight in ncTarget medium supplemented with 1 μM CHIR99021 (S1263, Selleck, US). From days 0–1, the medium was RPMI1640 (11875119, Thermo Fisher Scientific, US) supplemented with B27 insulin minus, 50 ng/mL Activin A (338-AC, R & D Systems, US), and 1/60 Matrigel (Growth Factor Reduced; 354230, BD, US). From days 1–2, the medium was changed to RPMI 1640 supplemented with B27 insulin minus, 40 ng/mL BMP4, and 1 μM CHIR99021. From days 2–5, the medium was changed to Vivo15 (BE02-060F, Lonza, Switzerland) supplemented with ITS (I3146, Merck, US), 500 μM monothioglycerol (M6145, Sigma-Aldrich), GlutaMax (35050061, Gibco), 50 μg/mL ascorbic acid (A8960, Sigma-Aldrich), 0.1% bovine serem albumin (BSA; V900933, Sigma-Aldrich), 300 ng/

mL vascular endothelial growth factor (VEGF; 293-VE, R & D Systems), 5 ng/mL FGF2 (96-100-18B, PeproTech), and 10 ng/mL BMP4. On day 5, we obtained endothelial progenitor cells to generate LOs.

For hepatic lineage differentiation of human iPSCs, cells were seeded onto Matrigel-coated plates in ncTarget medium and cultured overnight. From days 0–1, the medium was RPMI1640 supplemented with B27 insulin minus and 3 μM CHIR99021. From days 2–3, the medium was changed to RPMI 1640 supplemented with B27 insulin minus and 100 ng/mL Activin A. From days 5–8, the medium was changed to RPMI 1640 supplemented with B27 (A1486701, Gibco), 20 ng/mL BMP4, and 10 ng/mL FGF2 for hepatoblast induction. On day 8, we obtained hepatoblast cells to generate LOs.

2.2. The assessment of induced pluripotent stem cell-derived hepatic stellate cell activation

To assess activation competence, day 12 iPSC-derived HSCs were exposed to recombinant transforming growth factor-beta 1 (TGF-β1; 240-B, R & D Systems) at 10 ng/mL for 24 h. Activation was determined by immunostaining for alpha-smooth muscle actin (α-SMA) and analysis of fibrosis-associated gene expression. Morphological changes during extended culture were documented by fluorescence imaging through day 14.

Spontaneous autofluorescence of day 12 HSCs was examined as a functional feature associated with HSC maturation. Fluorescence was imaged using a laser-scanning confocal microscope (LSCM; C2, Nikon, Japan) at 340 nm under filter settings, and changes during continued culture were qualitatively compared with the emergence of a fibrotic phenotype.

2.3. Assembly of multicellular liver organoids with induced pluripotent stem cell-derived hepatic stellate cells

To determine the optimal differentiation stage of iPSC-derived HSCs for organoid assembly, HSCs harvested on day 10 or day 12 were combined with endothelial cells and hepatocyte-lineage cells to generate multicellular aggregates in AggreWell plates (34415, STEMCELL Technologies, Canada). Single-cell suspensions were prepared via dissociation with Accutase (07920, STEMCELL Technologies). The three cell populations were subsequently combined at a stoichiometric ratio of 1:1:1 (HSCs:endothelial cells:hepatoblasts) to ensure uniform multicellular integration.

Cells were seeded into microwells and maintained in a specialized organoid culture medium. This basal medium consisted of a 1:1:1 mixture of Dulbecco's Modified Eagle Medium (DMEM)/F-12 (11320033, Gibco), Medium 199 (11150059, Gibco), and William's E Medium (12551032, Gibco), supplemented with 500 μM monothioglycerol, B27, 1% ITS, 50 μg/mL ascorbic acid, 0.1% BSA, 2% fetal bovine serum, 1% sodium pyruvate (P2256, Sigma-Aldrich), 1% minimum essential medium non-essential amino acids, 1% GlutaMAX, 20 ng/mL VEGF, 20 ng/mL hepatocyte growth factor (HGF; 96-100-39, PeproTech), 20 ng/mL Oncostatin M (96-300-10, PeproTech), and 5 ng/mL FGF2. The medium was refreshed every other day.

2.4. Hydrogel preparation and rheological characterization

To investigate the role of matrix viscoelasticity in regulating LO behavior, two DLP-printable hydrogel systems were prepared with comparable stiffness but distinct stress-relaxation properties: 1% PEG10000DA (455008, Sigma-Aldrich)–5% gelatin methacryloyl (GelMA; EFL-GM-60, EFL Global, Sri Lanka), and 1% F127DA (EFL-F127Dam EFL)–5% GelMA. PEG10000DA, F127DA, and GelMA were dissolved in Dulbecco's phosphate-buffered saline (DPBS) containing 16 mM lithium phenyl-2,4,6-trimethylbenzoylphosphinate (LAP; 900889, Sigma-Aldrich) and 0.8 mM Tartrazine (T0388, Sigma-Aldrich).

Mechanical properties were measured using a rheometer (MCR302e, Anton Paar, Austria). Briefly, the rheometer was equipped with a cone plate with a 25 mm diameter, a 99 μm truncation gap, and a 2° cone angle. The platform temperature was set at 37 °C. The storage modulus (G′) was determined under oscillatory shear at 1 Hz. Stress-relaxation testing was performed by applying a constant strain of 5% and recording stress decay over time. The linear limit of the strain was analyzed using the Analysis Window in RheoPlus software (Version 1.34, Anton Paar) with a smoothing range of 5% to obtain the G′ and G″ values under different conditions. Hydrogels with matched G′ but distinct relaxation profiles were selected for subsequent studies. Under these conditions, poly(ethylene glycol) diacrylate (PEGDA)–GelMA behaved as a slow-relaxing matrix, whereas F127DA–GelMA exhibited rapid stress relaxation.

2.5. Encapsulation of liver organoids in hydrogels

Preformed LOs were resuspended in hydrogel precursor solutions and encapsulated by photocrosslinking using a DLP-based printing or light-curing system (LUMEN X+, CELLINK, Sweden). Crosslinking was performed for 4 s and 30 mW/cm^2 of 405 nm under sterile conditions. Organoid-laden constructs were maintained in organoid culture medium for two days. The transplanted LOs were approximately 100 μm in size, with approximately 100 organoids per mouse.

Organoid morphology within the hydrogels was evaluated using brightfield and fluorescence microscopy (Nikon Eclipse Ti2-E with an AX confocal module; FITC/TRITC/DAPY, Nikon, Japan). Morphological parameters, including organoid compaction, outward migration, and interaction with the surrounding matrix, were assessed qualitatively using NIS-Elements AR (Nikon). To determine the effect of matrix relaxation on HSC-associated transcriptional programs, RNA was isolated from encapsulated organoids after two days of culture and analyzed using quantitative reverse transcription polymerase chain reaction (qRT–PCR) for *PDGFRB*, *HGF*, *GFAP*, *LOXL2*, *ACTA2*, and *TIMP1*.

2.6. Digital light processing bioprinting of macroencapsulated liver organoid constructs

For macroencapsulation, a core–shell construct was designed using 14% F127DA–5% GelMA as the outer protective layer and 1% F127DA–5% GelMA as the inner cell-laden compartment containing LOs. Printing was performed using a DLP bioprinter (LUMEN X+) under sterile conditions. Printing parameters, including a layer thickness of 100 μm, an exposure time of 4 s per layer at a light intensity of 20 mW/cm^2, and a cumulative light dose of 80 mJ/cm^2 per layer, were optimized to balance structural fidelity and cell survival. Construct integrity was assessed immediately after printing through gross inspection and microscopy.

2.7. Subcutaneous implantation and histological analysis

All animal experiments were approved by the Institutional Animal Care and Use Committee (MDL2024-09-27-01) and performed in accordance with relevant institutional guidelines. A total of 40 immunocompetent male C57BL/6 mice (4 weeks old; Spefu Biotechnology Co., Ltd., China) were used for subcutaneous implantation studies.

To evaluate in vivo material stability, acellular hydrogels with identical morphology composed of 8% F127DA–5% GelMA or 14% F127DA–5% GelMA were implanted subcutaneously. At 14 days post-implantation, implants were retrieved and assessed for gross retention and degradation. Explanted tissues and major organs of the mice were fixed in 4% paraformaldehyde (PFA; 158127, Sigma-Aldrich), embedded in paraffin (P3558, Sigma-Aldrich), sectioned, and stained with hematoxylin and eosin (H & E; HHS316, Sigma-Aldrich) and Masson's trichrome (HT15, Sigma-Aldrich) to evaluate host response, collagen deposition, and fibrotic encapsulation.

For transplantation studies, bioprinted organoid-containing core–shell constructs were implanted subcutaneously using the same procedure. At the indicated endpoint, constructs were harvested for histology, viability assessment, and immunostaining. Fibrotic activation within explanted constructs was evaluated by staining for α-SMA (ab5694, Abcam, United Kingdom).

2.8. Fluorescent live/dead staining

Fluorescent live/dead staining was used to evaluate cell viability. Briefly, specimens were incubated in the dark for 15 min with 1 μM Calcein-AM (17783, Sigma-Aldrich) and 2 μM propidium iodide (P4170, Sigma-Aldrich) to stain live (green) and dead cells (red). An LSCM was used to acquire the images. The Image-Pro-Plus 6.0 (Media Cybernetics, US) count/size tool was used to quantify live and dead cells.

2.9. Immunofluorescence staining

Samples were fixed with 2.5% glutaraldehyde (G5882, Sigma-Aldrich), permeabilized with 0.1% Triton-X 100 (T8787, Sigma), blocked with 10% BSA, and then incubated with primary antibodies: activated leukocyte cell adhesion molecule (ALCAM; #MAB6561, R & D Systems), platelet-derived growth factor receptor beta (PDGFRβ; #ab32570, Abcam), α-SMA (#A5228, Sigma-Aldrich), neural cell adhesion molecule (NCAM; #AB5032, Sigma-Aldrich), reelin (RELN; #SAB4200453, Sigma-Aldrich), collagen type I alpha 1 chain (COL1A1; #C2456, Sigma-Aldrich), at 4 °C overnight, followed by incubation with the corresponding secondary antibody. Negative controls were obtained by replacing the primary antibodies with corresponding immunoglobulin G antibodies. Hoechst (H3570, Invitrogen, US) or 4',6-diamidino-2-phenylindole (DAPI; D9542, Sigma-Aldrich) was used to visualize the cell nuclei. LSCM was used to obtain the images.

2.10. Quantitative reverse transcription polymerase chain reaction assay

Quantitative reverse transcription polymerase chain reaction was performed to determine gene expression (Table S1). Briefly, cells were harvested from the liver models, and total RNA was extracted with TRIzol (Invitrogen). A complementary DNA synthesis kit (6210, Takara, Japan) was used for reverse transcription according to the manufacturer's instructions, and qRT-PCR was performed on a real-time PCR detection platform (CFX96, Bio-Rad, US) with Maxima SYBR Green qPCR master mix (Thermo Fisher Scientific). Each sample was analyzed in triplicate. The housekeeping gene glyceraldehyde-3-phosphate dehydrogenase (*GAPDH*) was used as an internal control for normalization.

2.11. Statistical analysis

Data are presented as mean ± SD, as indicated in the figure legends. All experiments were performed with at least three independent biological replicates. Statistical analyses were performed using GraphPad Prism 9.5 (GraphPad Software, US). Two-group comparisons were performed using two-tailed unpaired Student's *t*-tests. Multiple-group comparisons were analyzed using one-way ANOVA with Tukey's post hoc test. Differences were considered statistically significant if $p < 0.05$, as shown in the figure legends.

3. Results

3.1. Differentiation and activation of induced pluripotent stem cell-derived hepatic stellate cells

We first differentiated iPSCs into HSCs (Figure 1A). During the differentiation process, we observed a significant upregulation of *KDR* transcriptional expression during the mesodermal stage (days 0–4), followed by increased expression of *P75NTR*, *ALCAM*, *VIM*, and *PCDH7* during the mesenchymal and mesothelial cell stages (days 4–8) (Figure 1B and 1C). Furthermore, negative expression of stage-specific embryonic antigen-4 (SSEA4) and positive expression of ALCAM indicated successful differentiation into hepatic stellate progenitor cells (Figure 1C). By day 12, the transcriptional expression of *NCAM*, *PDGFRB*, *RELN*, *HGF*, *COL1A1*, *ACTA2*, and *PPARG* was significantly upregulated (Figure 1B), along with positive expression of HSC identity marker PDGFRβ and ALCAM (Figure 1C). We found that most cells at day 12 remained quiescent, with only subtle α-SMA expression compared with fibroblasts (Figure 1C). Additionally, day 12 cells can be activated by TGF-β, showing increased α-SMA expression (Figure 1D, 1E, and S1), indicating their responsiveness to fibrotic stimuli. However, prominent fibrosis was observed at day 14, with increased α-SMA expression, suggesting that HSCs could not maintain a quiescent state for extended periods under the current culture conditions (Figure 1D and 1E). Furthermore, spontaneous fluorescence of HSCs on day 12, a hallmark of functional maturity, diminished with extended culture (Figure 1F), indicating that iPSC-derived HSCs underwent fibrosis in culture, which complicated their use for applications requiring quiescent HSCs (Figure 1G).

3.2. Induced pluripotent stem cell-derived immature hepatic stellate cells are suitable for organoid formation with a quiescent phenotype

After differentiating iPSCs into HSCs for 10 or 12 days, we co-cultured the HSCs with iPSC-derived endothelial cells or hepatocytes in Aggrewell plates (Figure 2A). These two types of iPSC-derived HSCs form compact cell aggregates, indicating a mesenchymal phenotype (Figure 2B). Immunostaining showed that the LOs containing iPSC-derived HSCs at day 10 (LOs_D10) expressed PDGFRβ and showed minimal α-SMA expression, indicating a more quiescent state. In contrast, LOs containing iPSC-derived HSCs at day 12 (LOs_D12) exhibited increased expression of α-SMA, indicating the activated state of HSCs (Figure 2B and S2). Gene expression analysis showed that LOs_D10 exhibited lower expression of fibrosis-related genes, including *ACTA2* and *TIMP1*, compared to LOs_D12 (Figure 2C). These results suggest that day 10 HSCs are better suited for generating physiological LOs, as they maintain a more quiescent phenotype.

3.3. Matrix stress relaxation regulates liver organoid morphology and hepatic stellate cell-associated gene expression

To explore the effect of matrix viscoelasticity on the active state of LOs_D10, we established two DLP-printable hydrogel systems with comparable stiffness but distinct stress-relaxation properties: 1% PEGDA–5% GelMA and 1% F127DA–5% GelMA (Figure 3A). Both hydrogels exhibited comparable storage modulus (G′) around 500 Pa within the physiological range of the liver extracellular matrix (Figure 3B). PEGDA–GelMA retained higher residual stress and behaved as a slow-relaxing matrix, whereas F127DA–GelMA exhibited a fast-relaxing profile (Figure 3C and 3D). When LOs_D10 was encapsulated in these matrices, we observed obvious differences in the morphology: LOs_D10 in slow-relaxing PEGDA–GelMA exhibited more pronounced outward migration (Figure 3E) and stronger interactions with the surrounding matrix (Figure 3F), while those in fast-relaxing F127DA–GelMA retained a compact spherical structure with reduced migration (Figure 3E) and weaker interfacial attachment (Figure 3F). By analyzing gene expression in LOs_D10, the fast-relaxing matrix upregulated genes associated with functional maturity, including *PDGFRB*, *HGF*, and *GFAP*, whereas the slow-relaxing matrix preferentially upregulated genes associated with HSC activation, such as *LOXL2*, *ACTA2*, and *TIMP1* (Figure 3G). These findings indicate that at modulus within the physiological range of the liver, fast-relaxing matrices promote a more quiescent phenotype, whereas slow-relaxing matrices mimic fibrotic environments that drive HSC activation.

3.4. Digital light processing-bioprinted hydrogel construct encapsulating liver organoid

To 3D print macroencapsulated hydrogels for in vivo transplantation of LOs, we first examined the structural integrity of F127DA–GelMA hydrogels at different

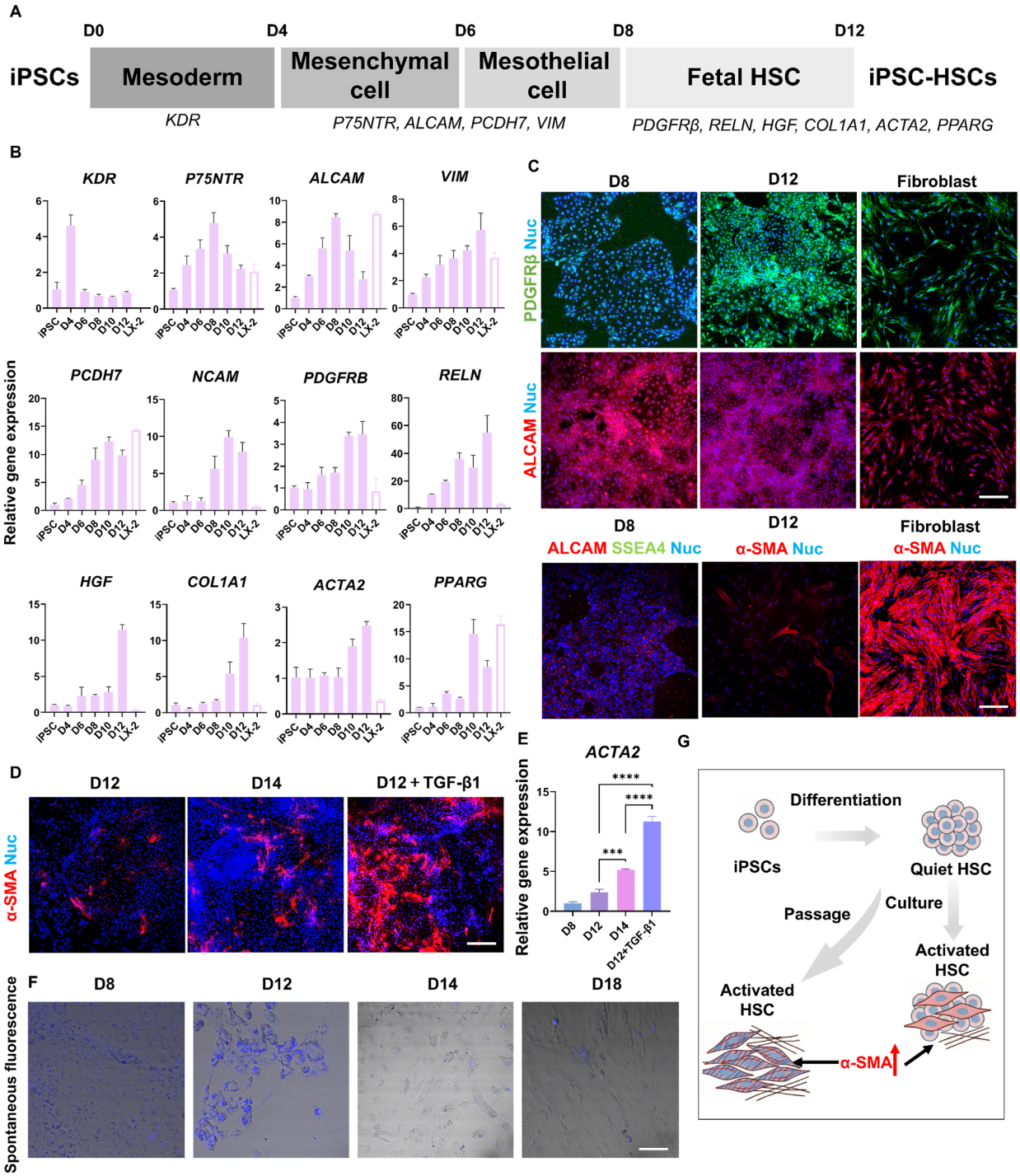

Figure 1. Stepwise differentiation and activation profiling of iPSC-HSCs. (A) Schematic of the differentiation trajectory from iPSCs to iPSC-HSCs. (B) Temporal expression of indicated lineage markers during differentiation. (C and D) Representative immunofluorescence images showing marker expression at the indicated stages and after TGF-β1 treatment. Three experimental groups are defined as follows: D12 represents day 12 of differentiation; D14 represents day 14 of differentiation; and D12+TGF-β1 represents cells at day 12 of differentiation treated with TGF-β1 for 24 h. Scale bars: 100 μm; magnifications: 20×. (E) Quantification of *ACTA2* expression. (F) Representative spontaneous fluorescence images during culture. Scale bar: 200 μm; magnification: 10×. (G) Schematic of iPSC-HSC differentiation, culture-dependent activation, and α-SMA upregulation.

Notes: Data are mean ± SD. $^{***}p < 0.001$, $^{****}p < 0.0001$.

Abbreviations: α-SMA: Alpha-smooth muscle actin; ALCAM: Activated leukocyte cell adhesion molecule; HSC: Hepatic stellate cell; iPSC: Induced pluripotent stem cell; Nuc: Nucleus; PDGFRβ: Platelet-derived growth factor receptor beta; TGF-β1: Transforming growth factor-beta 1.

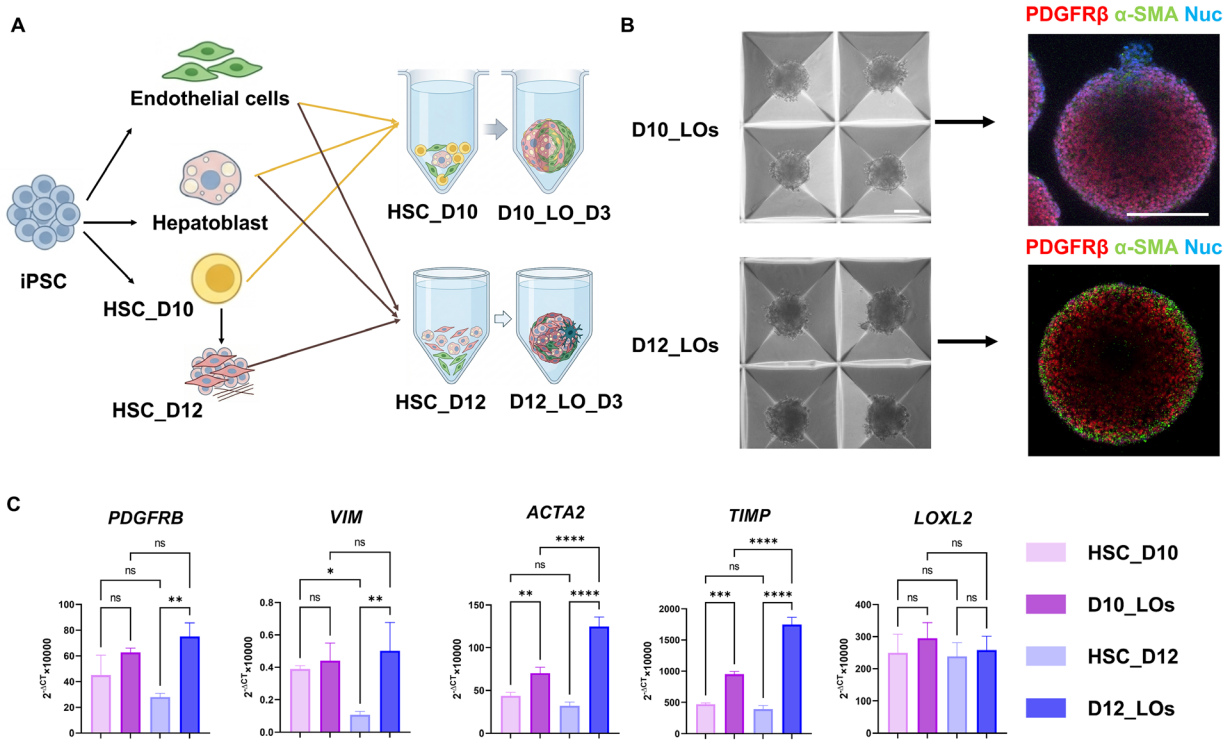

Figure 2. iPSC-derived HSCs at day 10 are suitable for organoid formation with a quiescent phenotype. (A) Schematic of iPSC differentiation into HSCs and co-culture with endothelial or hepatocyte cells in 3D conditions. (B) Morphology of days 10 and 12 HSCs cultured in 3D matrices (D10_LOs and D12_LOs). Immunofluorescence images showing PDGFRβ (red) and α-SMA (green). Scale bars: 50 μm; magnifications: 40×. (C) Gene expression analysis of HSC markers.

Notes: Data are mean ± SD. ns: Not significant; $^{*}p < 0.05$, $^{**}p < 0.01$, $^{***}p < 0.001$, $^{****}p < 0.0001$.

Abbreviations: α-SMA: Alpha-smooth muscle actin; HSC: Hepatic stellate cell; iPSC: Induced pluripotent stem cell; LO: Liver organoid; Nuc: Nucleus; PDGFRβ: Platelet-derived growth factor receptor beta.

concentrations following subcutaneous implantation in immunocompetent mice. By day 14, 8% F127DA–GelMA had undergone substantial degradation, leaving minimal residual material, whereas 14% F127DA–GelMA maintained its structure without significant degradation or signs of inflammation (Figure 4A). Histological analysis confirmed greater hydrogel retention in the 14% F127DA–GelMA group, with no notable collagen deposition or fibrotic encapsulation around the implant (Figure 4B and S3). This long-term stability and low fibrosis are critical for supporting cell transplantation in immunocompetent mice. We did not observe any obvious pathological changes in the organs of mice 14 days after transplantation with 14% F127DA–GelMA (Figure S4). Based on these results, we designed a composite bioprinted construct consisting of an outer protective shell of 14% F127DA–5% GelMA and an inner compartment of 1% F127DA–5% GelMA mimicking an extracellular matrix to encapsulate day 10 LOs (Figure 4C). The printed constructs exhibited robust structural integrity and high cell viability (Figure 4D). Following subcutaneous implantation, the constructs remained intact and localized at the implantation site for at least 14 days (Figure 4E), maintained cell viability (Figure 4F), and showed no significant increase in α-SMA expression, indicating that LOs_D10 maintained a quiescent phenotype (Figure 4G). These results support the use of the F127DA–GelMA DLP bioprinting platform as a biocompatible macroencapsulation strategy for in vivo delivery of iPSC-derived LOs in immunocompetent hosts.

4. Discussion

We established a DLP-printable LO platform that addresses the challenge of maintaining HSC quiescence in mechanically sensitive constructs. By integrating stage-selected iPSC-derived HSCs, a fast stress-relaxing hydrogel, and macroencapsulation, we generated spatially defined, transplantable organoids that preserve HSC low-activation states while enabling high-fidelity printing and structural

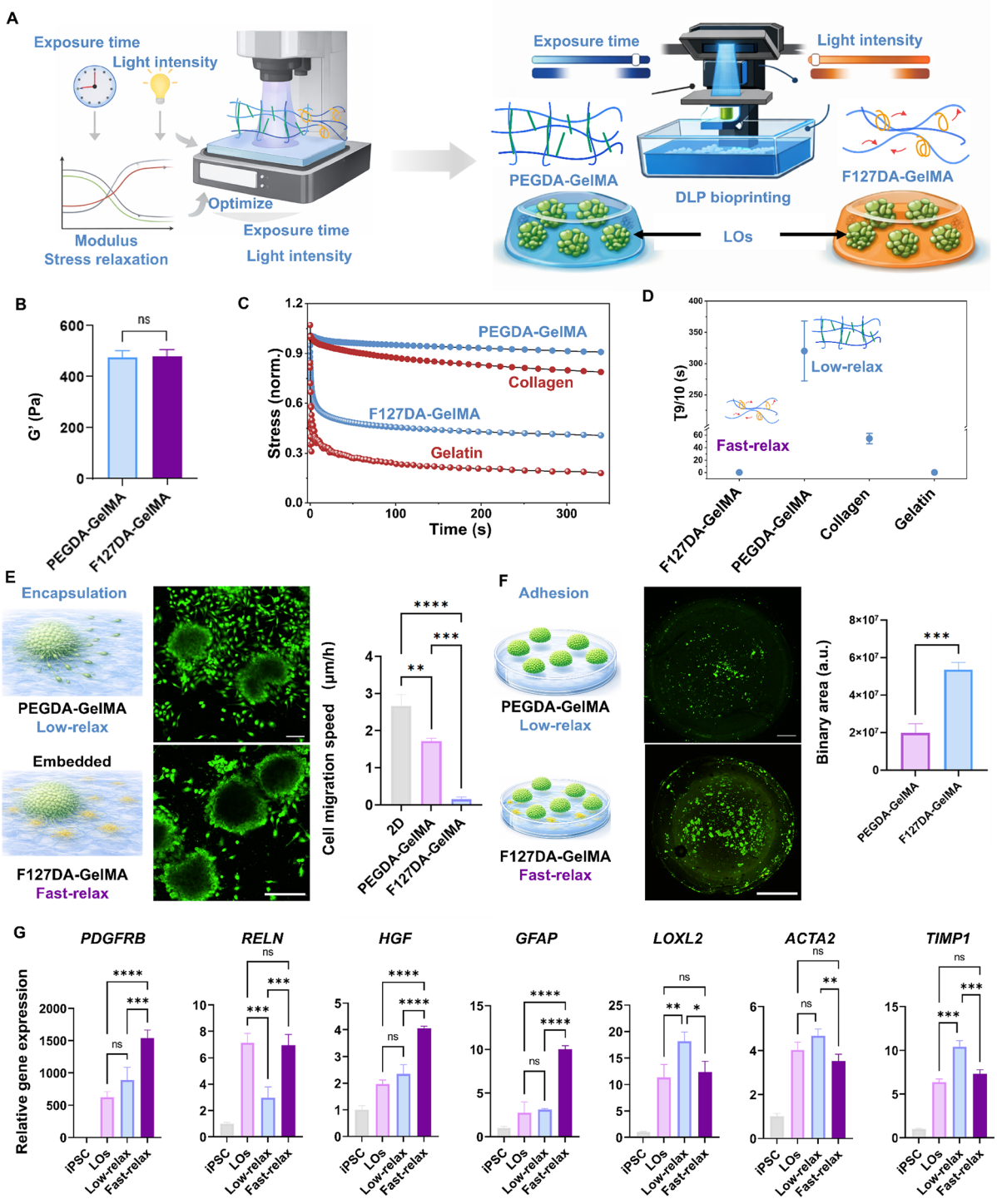

Figure 3. Hydrogel viscoelasticity regulates LOs behavior. (A) Schematic of photorheology-guided hydrogel optimization and DLP bioprinting. (B) Storage modulus (G′) of hydrogels. (C and D) Stress-relaxation curves and quantification. (E and F) Representative images and quantification of cell migration. Scale bars: 200 μm; magnifications: 10×. (G) Relative expression of genes.

Notes: Data are mean ± SD. ns: Not significant; $^{**}p < 0.01$, $^{***}p < 0.001$, $^{****}p < 0.0001$.

Abbreviations: DLP: Digital light processing; GelMA: Gelatin methacryloyl; LO: Liver organoid; norm.: Normalized; PEGDA: Poly(ethylene glycol) diacrylate.

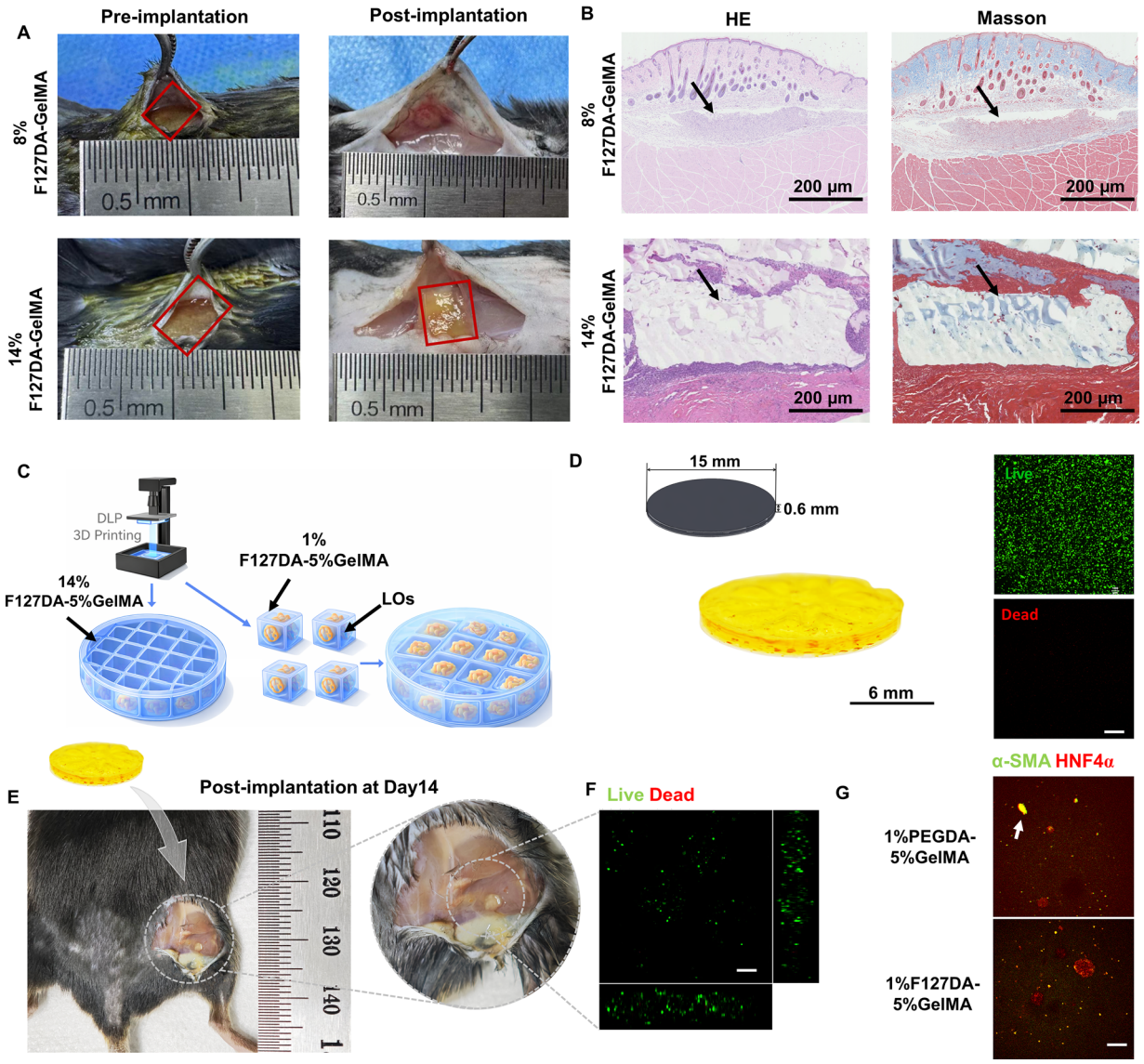

Figure 4. In vivo validation of bioprinted hydrogels and liver organoids. (A and B) Gross images and histology of implanted hydrogels at indicated compositions. Scale bars: 200 μm; magnifications: 10×. (C) Schematic of DLP bioprinting and encapsulation of LOs_D10. Representative images of (D, E) printed constructs and live/dead staining after (D) printing and (F) implantation. Scale bars: 200 μm; magnifications: 10×. (G) Representative histological analysis of implanted constructs. Scale bar: 100 μm; magnification: 20×.
Abbreviations: α-SMA: Alpha-smooth muscle actin; DLP: Digital light processing; HE: Hematoxylin and eosin; HNF4α: Hepatocyte nuclear factor 4 alpha; GelMA: Gelatin methacryloyl; LO: Liver organoid; PEGDA: Poly(ethylene glycol) diacrylate.

stability. This approach overcomes the mechanical stresses inherent to DLP bioprinting and provides a practical strategy for building organoid constructs suitable for in vivo transplantation.

Hepatic stellate cells are increasingly recognized as regulators of liver zonation, regeneration, metabolism, and organoid maturation, rather than merely fibrogenic effector cells.[5] Pluripotent stem cells can be differentiated into quiescent HSC-like cells, providing a practical human cell source that helps overcome the limited availability of primary cells.[7] Our results support the reproducibility of this differentiation strategy across laboratories, but also highlight an important limitation. Although day 12 iPSC-derived HSCs displayed features associated with HSC maturation, this state was transient and readily shifted toward activation with continued culture. Compared with

day 12 cells, day 10 iPSC-derived HSCs retained HSC identity, supported multicellular organoid assembly, and showed lower expression of fibrosis-associated genes. These findings suggest that the most suitable HSC population for building physiological LOs is not necessarily the most mature, but rather the one least prone to activation during subsequent culture.

To better preserve organoid quiescence after DLP printing, we sought to define the relevant mechanical features of the hydrogel. PEGDA–GelMA and F127DA–GelMA were selected to provide comparable initial stiffness but distinct stress-relaxation profiles. Both PEGDA and F127DA are widely used synthetic polymers that are relatively bioinert and lack intrinsic cell-adhesive motifs[16,17], whereas GelMA provides cell-interactive sites such as RGD sequences. Since both formulations contained the same GelMA concentration, the major bioactive ligand component was kept comparable between groups, while PEGDA and F127DA mainly served as tunable network-forming components. By comparing hydrogels with matched stiffness but distinct stress-relaxation profiles, we identified stress relaxation as an independent regulator of the LO state. Slow-relaxing PEGDA–GelMA promoted outward migration and higher expression of activation-associated genes, whereas fast-relaxing F127DA–GelMA preserved compact morphology and favored quiescence-associated markers. Previous work reported that relaxation of matrix mechanics can partially, although incompletely, reverse HSC activation.[18] These results suggest that matrix stress relaxation is closely associated with HSC phenotype regulation, beyond the effect of initial stiffness alone. As recent reviews have emphasized, printing-compatible materials should support not only structural fidelity but also functional homeostasis.[9] Our results therefore suggest that, in printable LO systems, hydrogel design for HSC-containing constructs should account not only for stiffness but also for force dissipation. Nevertheless, PEGDA–GelMA and F127DA–GelMA are not chemically identical. Future studies using chemically matched or independently tunable viscoelastic hydrogels will be needed to more precisely define the role of relaxation kinetics in HSC fate regulation.

For DLP-printed constructs intended for implantation, sufficient mechanical support is required to maintain structural integrity during handling and after implantation, which often necessitates a relatively high modulus.[19] This poses a particular challenge for LOs containing HSCs that are sensitive to mechanical cues. To address this, we used DLP printing to spatially separate mechanical and biological functions by constructing a mechanically supportive outer hydrogel shell and an inner hydrogel compartment encapsulating the organoids. In our system, the fast-relaxing inner matrix preserved quiescence-associated features without an immediate increase in α-SMA, while the supportive outer hydrogel shell enabled implantation in immunocompetent mice. Although we have not yet assessed long-term functional outcomes, these results suggest that an organoid state established through stress-relaxation-guided matrix selection can withstand DLP fabrication, macroencapsulation, and implantation in immunocompetent hosts without immediately drifting toward α-SMA-associated fibrotic activation. Compared with previous encapsulation-based studies, our system extends this concept to multicellular LOs containing HSCs and emphasizes preservation of HSC quiescence.[20]

A limitation of this study is the lack of longer-term in vivo investigations to determine whether these constructs can maintain graft stability, hepatocyte-specific functions, vascularization, immune infiltration, fibrotic capsule maturation, and sustained LO phenotype. Nevertheless, our work establishes a feasible framework for generating bioprinted and transplantable human LOs. This framework emphasizes the maintenance of a low-activated HSC baseline throughout cell selection, matrix design, and subsequent implantation.

5. Conclusion

We developed a DLP-bioprinted macroencapsulation system for human LOs that maintained stellate cells in a low-activation state. Day 10 iPSC-derived HSCs were more suitable for organoid assembly than day 12 cells, and fast stress-relaxing hydrogels better preserved organoid morphology and quiescence-related features than stiffness-matched slow-relaxing matrices. The core–shell construct demonstrated high viability and remained stable after implantation in immunocompetent mice, providing a practical basis for the development of transplantable LOs and for future functional evaluation studies.

Acknowledgments

None.

Funding

This work was supported by the National Natural Science Foundation of China (22534006) and the Tianjin Natural Science Foundation Project (23JCQNJC00790).

Conflict of interest

The authors declare that they have no known competing financial interests or personal relationships that could have appeared to influence the work reported in this paper.

Author contributions

Conceptualization: Zhi Zhou, Xiaodong Ding
Formal analysis: Ruitong Li, Xiaodong Ding
Investigation: Zhi Zhou, Ruitong Li, Xiaodong Ding
Methodology: Ruitong Li, Xiaodong Ding, Yixuan Li
Writing–original draft: Shaojun Liang
Writing–review & editing: Ruitong Li, Yixue Luo

Ethics approval and consent to participate

All animal experiments were approved by the Institutional Animal Care and Use [MDL2024-09-27-01] and performed in accordance with relevant institutional guidelines.

Consent for publication

Not applicable.

Availability of data

The data are available from the corresponding author upon reasonable request.

References

1. Takebe T, Sekine K, Enomura M, *et al.* Vascularized and functional human liver from an iPSC-derived organ bud transplant. *Nature*. 2013;499(7459):481-484.

   doi: 10.1038/nature12271

2. Tang XY, Wu S, Wang D, *et al.* Human organoids in basic research and clinical applications. *Signal Transduct Target Ther*. 2022;7(1):168.

   doi: 10.1038/s41392-022-01024-9

3. Harrison SP, Baumgarten SF, Verma R, Lunov O, Dejneka A, Sullivan GJ. Liver Organoids: Recent Developments, Limitations and Potential. *Front Med*. 2021;8:574047.

   doi: 10.3389/fmed.2021.574047

4. Grebenyuk S, Abdel Fattah AR, Kumar M, *et al.* Large-scale perfused tissues via synthetic 3D soft microfluidics. *Nat Commun*. 2023;14(1):193.

   doi: 10.1038/s41467-022-35619-1

5. Kamm DR, McCommis KS. Hepatic stellate cells in physiology and pathology. *J Physiol*. 2022;600(8):1825-1837.

   doi: 10.1113/JP281061

6. Trivedi P, Wang S, Friedman SL. The Power of Plasticity-Metabolic Regulation of Hepatic Stellate Cells. *Cell Metab*. 2021;33(2):242-257.

   doi: 10.1016/j.cmet.2020.10.026

7. Coll M, Perea L, Boon R, *et al.* Generation of Hepatic Stellate Cells from Human Pluripotent Stem Cells Enables In Vitro Modeling of Liver Fibrosis. *Cell Stem Cell*. 2018;23(1):101-113.e7.

   doi: 10.1016/j.stem.2018.05.027

8. Koui Y, Himeno M, Mori Y, *et al.* Development of human iPSC-derived quiescent hepatic stellate cell-like cells for drug discovery and in vitro disease modeling. *Stem Cell Rep*. 2021;16(12):3050-3063.

   doi: 10.1016/j.stemcr.2021.11.002

9. Huang MS, Christakopoulos F, Roth JG, Heilshorn SC. Organoid bioprinting: from cells to functional tissues. *Nat Rev Bioeng*. 2024;3(2):126-142.

   doi: 10.1038/s44222-024-00268-0

10. Zhao Z, Chen X, Dowbaj AM, *et al.* Organoids. *Nat Rev Methods Primers*. 2022;2:94.

    doi: 10.1038/s43586-022-00174-y

11. Ding H, Dong M, Zheng Q, Wu ZL. Digital light processing 3D printing of hydrogels: a minireview. *Mol Syst Des Eng*. 2022;7(9):1017-1029.

    doi: 10.1039/d2me00066k

12. Jeong YG, Yoo JJ, Lee SJ, Kim MS. 3D digital light process bioprinting: Cutting-edge platforms for resolution of organ fabrication. *Mater Today Bio*. 2024;29:101284.

    doi: 10.1016/j.mtbio.2024.101284

13. Duong VT, Lin CC. Digital Light Processing 3D Bioprinting of Gelatin-Norbornene Hydrogel for Enhanced Vascularization. *Macromol Biosci*. 2023;23(12):e2300213.

    doi: 10.1002/mabi.202300213

14. Zhu S, Liao X, Xu Y, *et al.* 3D bioprinting of high-performance hydrogel with in-situ birth of stem cell spheroids. *Bioact Mater.* 2025;43:392-405.

    doi: 10.1016/j.bioactmat.2024.09.033

15. He N, Wang X, Shi L, *et al.* Photoinhibiting via simultaneous photoabsorption and free-radical reaction for high-fidelity light-based bioprinting. *Nat Commun*. 2023;14(1).

    doi: 10.1038/s41467-023-38838-2

16. Zhu J. Bioactive modification of poly(ethylene glycol) hydrogels for tissue engineering. *Biomaterials*. 2010;31(17):4639-4656.

    doi: 10.1016/j.biomaterials.2010.02.044

17. Zhao P, Wang B, Wang L, *et al.* Rapid printing of 3D porous scaffolds for breast reconstruction. *Bio-des Manuf*. 2023;6(6):691-703.

    doi: 10.1007/s42242-023-00253-3

18. Caliari SR, Perepelyuk M, Soulas EM, Lee GY, Wells RG, Burdick JA. Gradually softening hydrogels for modeling hepatic stellate cell behavior during fibrosis regression. *Integr Biol*. 2016;8(6):720-728.

    doi: 10.1039/c6ib00027d

19. Fowler M, Moreno Lozano A, Krause J, *et al.* Guiding

vascular infiltration through architected GelMA/PEGDA hydrogels: an *in vivo* study of channel diameter, length, and complexity. *Biomater Sci*. 2025;13(11):2951-2960.

doi: 10.1039/d5bm00193e

20. Wang Y, Huang R, Lu Y, Liu M, Mo R. Immuno-protective vesicle-crosslinked hydrogel for allogenic transplantation. *Nat Commun*. 2024;15(1):5176.

doi: 10.1038/s41467-024-49135-x